Supplementary Information for

Disproportionate increase in freshwater methane emissions induced by experimental warming

Yizhu Zhu[1], Kevin J Purdy[2], Özge Eyice[1], Lidong Shen[1,3], Sarah F Harpenslager[1,4], Gabriel Yvon-Durocher[5], Alex J. Dumbrell[6], Mark Trimmer[1]*

Affiliations:

[1]School of Biological and Chemical Sciences, Queen Mary University of London, London, E1 4NS, UK.

[2]School of Life Sciences, University of Warwick, Coventry, CV4 7AL, UK.

[3]Institute of Ecology, School of Applied Meteorology, Nanjing University of Information Science and Technology, Nanjing 210044, China.

[4]Leibniz Institute of Freshwater Ecology and Inland Fisheries (IGB), Department of Ecosystem Research, 12587, Berlin, Germany.

[5]Environment and Sustainability Institute, University of Exeter, Penryn Campus, Penryn, Cornwall, TR10 9FE, UK.

[6]School of Life Sciences, University of Essex, Colchester, Essex, U.K. CO4 3SQ.

This Supplementary Information includes:

Supplementary Discussion

The production of both CH_4 and CO_2 by a combination of acetoclastic and hydrogenotrophic methanogenesis in relation to Ralf Conrad's 1999 publication (Ref. 24 in main text)

Determining the absolute ratio of CH_4:CO_2 from any substrate via methanogenesis is challenging. Conrad (Ref. 24 in main text) calculated the idealised outcome of glucose degradation in a strictly methanogenic system, which does return a 1:1 ratio of CH_4 and CO_2, via 33% hydrogenotrophic and 67% acetoclastic methanogenesis. However, he then shows that this idealised ratio is rarely true in nature where a strictly methanogenic system simply does not exist (and *see* Ref. 28 and 34 cited in the main text). Indeed here, we have compiled CH_4 and CO_2 production data from 13 studies including wetlands[1–11], permafrost thaw[12] and lakes[13] which demonstrate that the vast majority of CH_4:CO_2 production ratios are less than 0.5 with a median of 0.28 only (*see* panel **a** in the figure below). Thus, in reality, Conrad's idealised ratio appears to be rare in natural systems and the same is true in our experimental ponds where the CH_4:CO_2 ratios are less than 1:1 in both the ambient and warmed ponds (0.2:1 *vs.* 0.7:1).

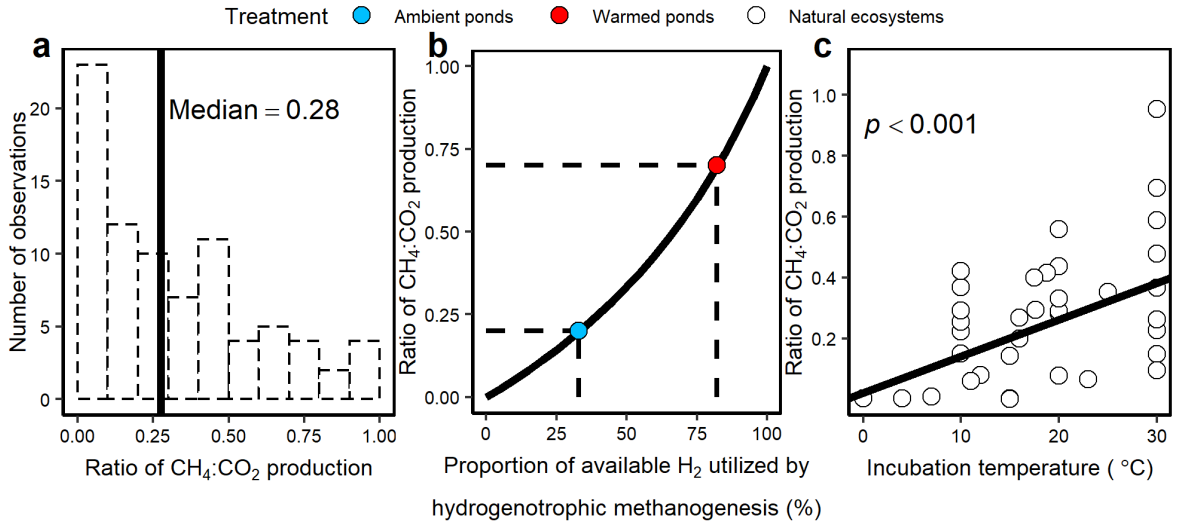

Given that the carbon quality is similar between the warmed and ambient ponds (*see* Fig. 2b in main text), why has the CH_4:CO_2 ratio increased after eleven years' warming? Here Conrad's model can be used to consider what a change in the CH_4 to CO_2 ratio might mean. Conrad's concept (ref. 24) through fermentation assumes that:

$$(R1)\ 2CH_2O + 2H_2O \rightarrow 2CO_2 + 4H_2$$

In most freshwater ecosystems where inorganic electron acceptors other than CO_2 are not available, hydrogenotrophic methanogenesis competes against homoacetogenesis for electrons from H_2. We can

assume that the proportion of available H_2 utilized by hydrogenotrophic methanogenesis is n ($0<n<1$) and by multiplying everything in hydrogenotrophic methanogenesis with n as a factor we get:

(R2) $n CO_2 + 4n H_2 \rightarrow n CH_4 + 2n H_2O$

The sum of reaction (R1) and (R2) is:

(R3) $2CH_2O + (2-2n)H_2O \rightarrow (4-4n)H_2 + (2-n)CO_2 + nCH_4$

The ratio of CH_4 to CO_2 produced is therefore $n/(2-n)$. The 1:1 ratio of CH_4 to CO_2 production occurs only when 100% of H_2 produced via fermentation (R1) is used up to reduce CO_2 to CH_4 (i.e., $n=1$), the CH_4:CO_2 production ratio is however < 1:1 when homoacetogenesis outcompetes hydrogenotrophic methanogenesis for H_2 and electrons flow to acetate rather than CH_4 ($n<1$). More importantly, (R3) predicts that the ratio of CH_4 to CO_2 increases exponentially as a function of the proportion of available H_2 being utilized by hydrogenotrophic methanogenesis (n) (*see* panel **b** in the figure above). As H_2 becomes more available at higher temperatures[13], should an increasing CH_4:CO_2 ratio with temperature be expected? Indeed, this hypothesis is validated by a positive correlation between incubation temperatures and CH_4:CO_2 ratios produced in anoxic wetland soils[1,6,8,14] (*see* panel **c** in the figure above). Therefore, an idealized 1:1 ratio is rare in reality but the CH_4:CO_2 ratio increases towards the idealized 1:1 ratio predicted by Conrad at higher temperatures.

Furthermore, now we can rationalize the disproportionate increase in CH_4:CO_2 production ratio seen in our long-term warmed ponds using the proportion of available H_2 being utilized by hydrogenotrophic methanogenesis. At lower temperatures, electrons flow to acetate and as a result methane production is dominated by acetoclasty[15] and only a minor proportion of available H_2 is utilized by hydrogenotrophic methanogenesis (30 %, the blue dot in panel **b**, *see* figure above). In contrast, as H_2 concentrations increase with temperature, which thermodynamically favours hydrogenotrophic methanogenesis, a larger proportion of electrons and carbon flow to CH_4 (80 %, the red dot in panel **b**, *see* figure above), ultimately increasing the CH_4 to CO_2 ratio closer towards the idealised ratio predicted by Conrad. In Figure 3d of the main text, we show clearly that hydrogenotrophic methanogenesis is favoured by warming and so conclude that, from whatever source, more of the available hydrogen is being directed more efficiently into methane in the warmed compared to the ambient ponds and that such disproportionate increase in CH_4:CO_2 ratio will probably occur in natural freshwaters as the Earth warms.

Supplementary Figures

Supplementary Fig. 1 | Magnitude and frequency of methane emission through ebullition events (*n*=198, 1.2% identified of the 16504 total chamber measurements using our two criteria) and exclusion of 7 other non-steady flux events – *see* Methods).
Ebullition in our ponds exports methane from the sediments to the atmosphere directly and therefore: **1,** should increase with enhanced methanogenesis under warming; and **2,** follow a similar seasonal pattern to diffusion. Indeed, in line with our enhanced methanogenesis under warming, the average magnitude of ebullition events **a,** was 3-fold greater in the warmed ponds (80 ng CH_4 per event versus 27 ng CH_4 per event in the ambient ponds, *t*-statistic, ***: $p<0.001$). In addition, the magnitude of ebullition events **b**, and their frequency **c,** peaked in summer, demonstrating a similar seasonal pattern to diffusional methane emissions (Extended Data Fig. 2). Ebullition events in our ponds have therefore been captured. However, ebullition contributed only 0.2% of total methane emissions in both warmed and ambient ponds. The magnitude of ebullition events was calculated using the maximum methane concentration in a chamber measurement - *see* equation (1) in Methods. Error bars are standard errors of the magnitude of an ebullition event.

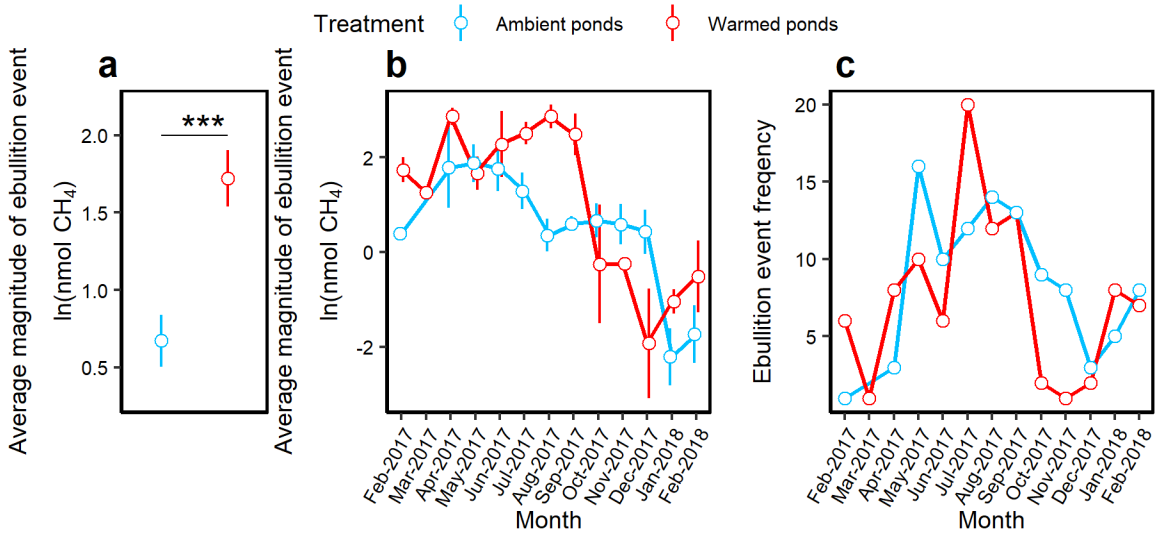

Supplementary Fig. 2 | Methanogen alpha diversity (*n*=79, monthly samples from April to August in 2016 from 8 ambient and 8 warmed ponds, *see* Methods). a, Observed OTUs, **b**, Shannon's diversity, **c**, Chao 1 diversity and **d**, evenness are all identical between the warmed (red) and ambient (blue) ponds. Statistical significance (P_{LRT}) was determined by a likelihood ratio test. Box lower and upper bounds are 25th and 75th percentiles, respectively, the line is the median. Whiskers indicate largest/smallest value no further than 1.5X the interquartile range. The data points (in magenta) beyond the end of whiskers are outliers.

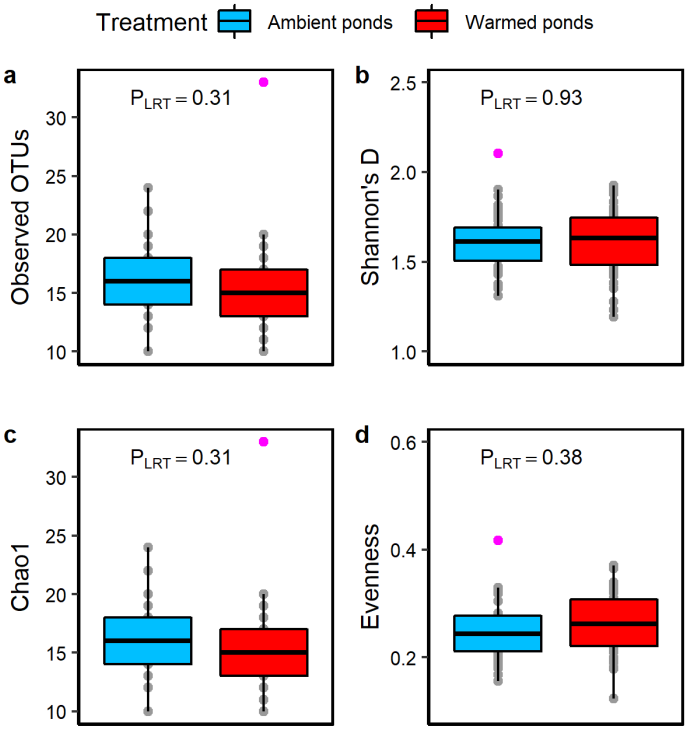

Supplementary Fig. 3 | Water column and sediment oxygen concentrations in the experimental ponds. a, Seasonality of the *in situ* dissolved oxygen concentrations in the overlying water of the warmed (red) and ambient (blue) ponds from October, 2015 to October, 2016 (n=5120, data collected at 10-minute intervals using oxygen sensor in 7 ambient and 7 warmed). **b**, Mean *in situ* dissolved oxygen concentration was lower in the warmed ponds compared to their ambient controls (n=5120, t-statistic, p<0.001). **c**, Oxygen penetration profiles measured in intact sediment cores at 15 °C (n=6, from 3 warmed and 3 ambient in April, 2016). Oxygen concentrations showed a steeper decline and penetrated to a shallower depth in the warmed pond sediment (4.86 mm) compared to 6.67 mm to the ambient pond sediments.

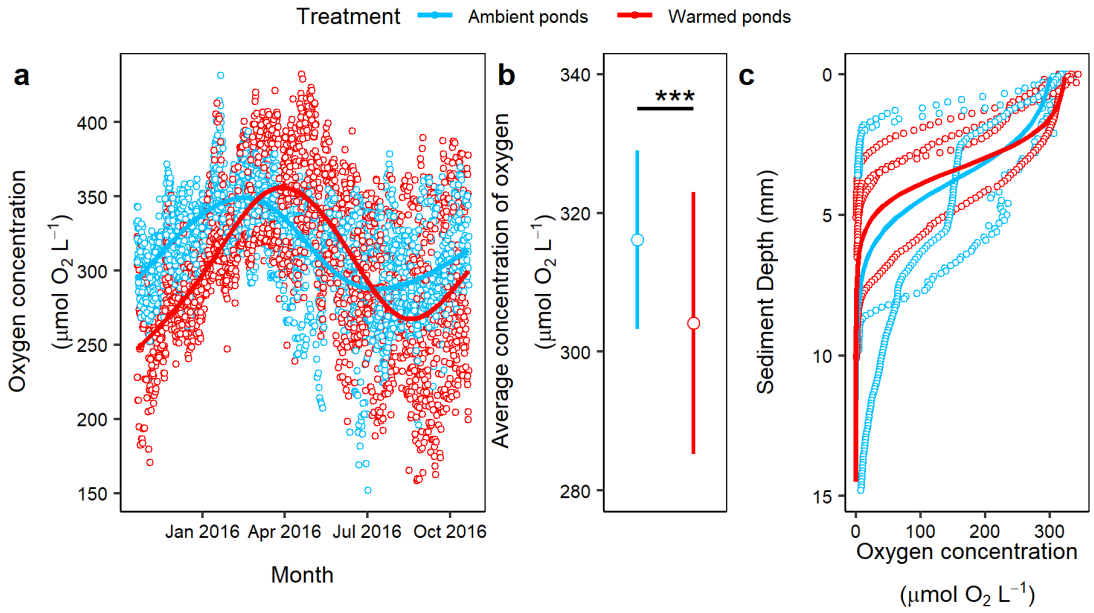

Supplementary Fig. 4 | Effect of long-term warming on the methanotroph community composition (*n*=80, monthly samples from March to July in 2017 from 8 ambient and 8 warmed ponds, *see* Methods). a, No overall change in the methanotroph community with long-term warming demonstrated by principal coordinate analysis (PCoA) using Bray-Curtis analysis and a Hellinger standardized dataset (at genus level) and **b**, differential abundance analysis at genus level detected no significant changes in any methanotroph genus.

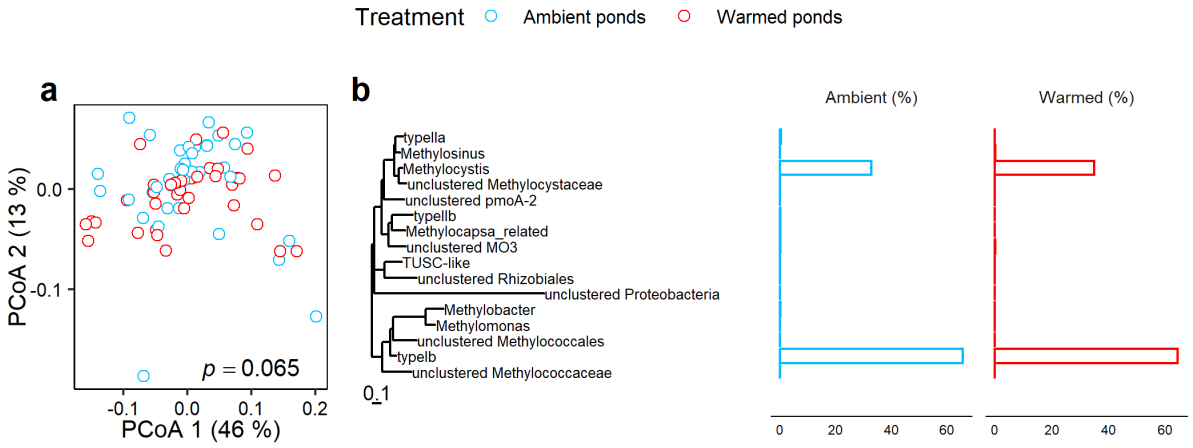

Supplementary Fig. 5 | Methanotroph alpha diversity (*n*=80, monthly samples from March to July in 2017 from 8 ambient and 8 warmed ponds, *see* Methods). a, Observed OTUs, **b**, Shannon's diversity, **c**, Chao 1 diversity and **d**, evenness are identical between the warmed (red) and ambient (blue) ponds. Statistical significance (P_{LRT}) was determined by a likelihood ratio test. Box lower and upper bounds are 25th and 75th percentiles, respectively, the line is the median. Whiskers indicate largest/smallest value no further than 1.5X the interquartile range.

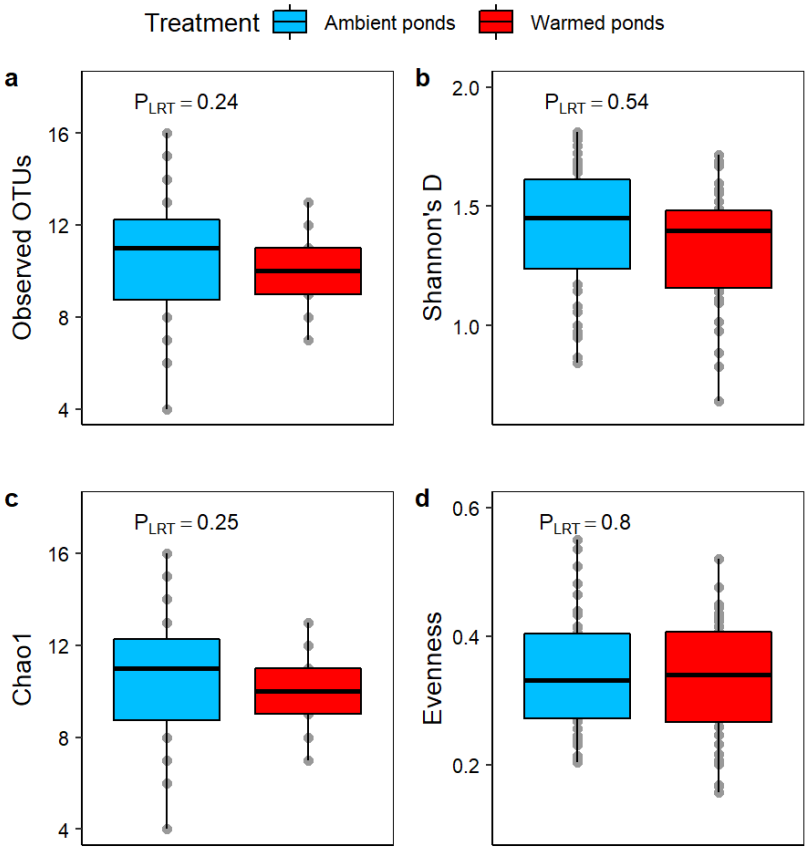

Supplementary Fig. 6 | Example of chamber measurements for a, steady-state flux b, strong ebullition and c, gentle ebullition. Chambers with a steady state flux (**a**) had standing methane concentrations of ~2 ppm. When a strong ebullition event occurred methane rose very rapidly to 30 ppm at ~ 4,000 ppb/s, while, in gentler ebullition events (**c**), methane concentrations could increase at 90 ppb/s to ~5 ppm. In both cases methane concentrations subsequently decreased more gently than the rapid increase.

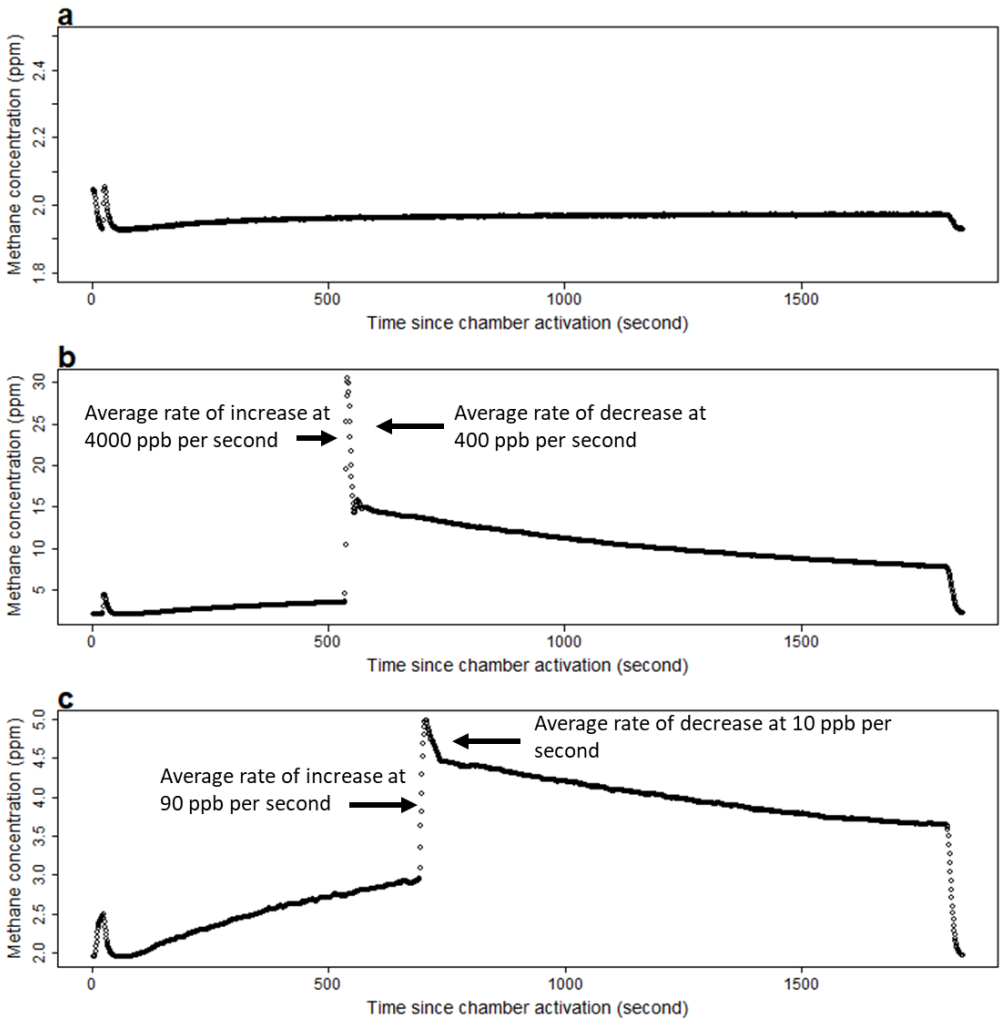

Supplementary Tables

Supplementary Table 1 | Original data sources for the analysis of methane emission capacities from globally distributed sites. Lat and Long represent latitude and longitude of each site. Avg. Temp = average annual temperature in each site. *n* represents the number of daily rate measurements of methane emissions for each site. The *p* values are less than 0.05 for each site, representing a good relationship between methane emission and air-temperature.

Site ID	Site Name	Lat	Long	Avg. Temp (°C)	Type	*n*	*p* value	
AT-Neu	Neustift	47.12	11.31	10.0	Grassland	539	<0.05	
CA-SCB	Scotty Creek Bog	61.31	-121.3	11.8	Wetland	639	<0.05	[16]
FR-LGt	La Guette	47.32	2.28	13.4	Wetland	215	<0.05	
US-CRT	Curtice Walter-Berger cropland	41.63	-83.35	7.2	Cropland	246	<0.05	[17]
US-EML	Eight Mile Lake Permafrost thaw gradient, Healy Alaska.	63.88	-149.25	3.6	Open shrubs	1015	<0.05	[18]
US-LA1	Pointe-aux-Chenes Brackish Marsh	29.50	-90.45	22.9	Wetland	206	<0.05	[19]
US-LA2	Salvador WMA Freshwater Marsh	29.86	-90.29	24.0	Wetland	531	<0.05	[20]
US-Los	Lost Creek	46.08	-89.98	6.9	Wetland	1499	<0.05	[21]
US-Myb	Mayberry Wetland	38.05	-121.77	17.1	Wetland	2687	<0.05	[22]
US-ORv	Olentangy River Wetland Research Park	40.02	-83.02	13.3	Wetland	1132	<0.05	[23]
US-OWC	Old Woman Creek	41.38	-82.51	20.3	Wetland	104	<0.05	[24]
US-PFa	Park Falls/WLEF	45.95	-90.27	6.9	Forest	975	<0.05	[25]
US-Sne	Sherman Island Restored Wetland	38.04	-121.76	16.1	Wetland	575	<0.05	[26]
US-StJ	St Jones Reserve	39.09	-75.44	18.0	Wetland	250	<0.05	[27]
US-Tw1	Twitchell West Pond Wetland	38.11	-121.65	18.6	Wetland	2039	<0.05	[28]
US-Tw4	Twitchell East End Wetland	38.10	-121.64	17.5	Wetland	1668	<0.05	[29]
US-Twt	Twitchell Island	38.11	-121.65	18.2	Cropland	351	<0.05	[30]
US-Uaf	University of Alaska, Fairbanks	64.87	-147.86	12.0	Forest	236	<0.05	[31]
US-WPT	Winous Point North Marsh	41.46	-82.99	11.3	Wetland	793	<0.05	[32]

Supplementary Table 2 | Annual methane budget, pond water characteristics and pond sediment characteristics.

		Ambient	Warmed	Ratio (W/A)
Production	Methane production capacity at 15 °C[1] (MG_{T15}, μmol CH_4 m^{-2} d^{-1})	2795 (1092)	7086 (2767)	2.5
	Effect of 4 °C warming predicted using the apparent activation energy $\overline{E_{MP}}$ ($Effect_{warming}$)[2]	1	1.5	1.5
	Methane production capacity (totMG)[3]	2795	10274	**3.7**
	mcrA abundance (log_{10}(copy g^{-1}(wet sediments)))	6.59 (0.045)	6.77 (0.034)	1.5
	Methanogen cell-specific activity (fmol CH_4 *mcrA*$^{-1}h^{-1}$)	0.35	0.59	1.7
Emission and proportion of CH_4 oxidized *in situ*	Annual methane emission (ME, μmol CH_4 m^{-2} d^{-1})	233 (22)	562 (63)	2.4
	Amount of methane oxidized *in situ*[4] (*in situ* totMO, μmol CH_4 m^{-2} d^{-1})	2563	9713	**3.8**
	Proportion of methane oxidized *in situ*[5] (MO%, %)	92	95	1.03
	Required proportion of CH_4 oxidized ($\%_{pred}$)[6]		**98**	
Oxidation	Kinetic effect of *in situ* methane concentrations ($Effect_{kinetic}$)[7]	1	1.9	1.9
	Effect of 4 °C warming predicted using apparent activation energy $\overline{E_{MO}}$ ($Effect_{warming}$)[2]	1	1.4	1.4
	Effect of sampling depth ($Effect_{sampling}$)[8]	1	1.4	1.4
	Methane oxidation capacity (*ex situ* totMO)[9]			**3.6**
	pmoA abundance (log_{10}(copy g^{-1}(wet sediments)))	3.99 (0.047)	4.38 (0.038)	2.45
	Predicted fold increase in *pmoA* abundance to offset warming-induced methane production (Ab_{pred})[10]			2.67
	Methanotroph cell-specific activity (pmol CH_4 *pmoA*$^{-1}h^{-1}$)	25.0	10.2	0.4
Water characteristic	Dissolved CH4 concentration (μmol L^{-1})	0.51 (0.15)	1.07 (0.21)	2.1
Sediment characteristic	Sediment % carbon	0.83 (0.089)	1.23 (0.13)	1.48
	Sediment % nitrogen	0.084 (0.0061)	0.11 (0.0010)	1.31
	Sediment C:N	9.37 (0.41)	10.40 (0.31)	1.11

Numbers given in the brackets are standard errors.

1. Methane production capacity at 15 °C was calculated by taking the exponential of the ln-transformed methane production rate in equation (4) ($\overline{lnF(T_C)}$) and converting from nmol g^{-1} h^{-1} to μmol m^{-2} d^{-1} (sediment density 1,068 Kg m^{-3} and depth 0.08 m) ($MG_{T15} = \overline{lnF(T_C)} \times 10^6 \times 24 \times 1.068 \times 10^6 \times 0.08$)

2. Effect of 4 °C warming on methane production and oxidation was calculated from the apparent activation energies: $\overline{E_{MP}}$ and $\overline{E_{MO}}$ for methane production and oxidation, respectively (*see* equations (2) and (4)). Apparent activation energies for methane production and oxidation in the warmed ponds are 0.7 eV and 0.57 eV, respectively, predicting a 1.5- and 1.4-fold increase in the methane production and oxidation, respectively.

3. In total, methane production capacity in the warmed ponds increased by 3.7-fold (totMG=MG_{T15}×$Effect_{warming}$).

4. Total methane oxidized *in situ* is the difference between methane production capacity and annual methane emission (i.e., *in situ* totMO = totMG - ME)

5. Proportion of oxidized methane is the percentage of methane emission to methane production capacity at annual average temperatures (i.e., MO% = (totMG -ME)/ totMG ×100%).

6. Proportion of methane oxidation required in the warmed ponds to prevent methane emissions from increasing (i.e., ($totMG_{warmed}$ – $ME_{ambient}$)/ $totMG_{warmed}$ ×100%).

7. Methane oxidation capacities at *in situ* methane concentrations were calculated using Michaelis-Menten model based on the methane concentrations in the pond water (*see* equation (7)).

8. Oxygen penetrated 4.86 and 6.67 mm into the warmed and ambient pond sediments, respectively (Supplementary Fig. 3). These depths were used as proxy for the active methanotrophy layer. Therefore, the effect of sampling the same depths in the warmed and ambient ponds for methane oxidation capacity measurements is $Effect_{sampling}=\frac{20\ mm}{4.86\ mm}/\frac{20\ mm}{6.67\ mm}$.

9. In total, warming increased the measured methane oxidation capacity in the warmed ponds by 3.6-fold ($Effect_{kinetic}$×$Effect_{warming}$×$Effect_{sampling}$), accounting for the discrepancy between predicted and measured methane emissions *in situ* (*ex situ* totMG = *in situ* totMO).

10. Warming has increased the methane oxidation capacity by 3.6-fold but not the 3.9-fold required to offset the greater warming-induced methane production (i.e., ($totMG_{warmed}$ – $ME_{ambient}$)/($totMG_{ambient}$ – $ME_{ambient}$)). Predicted methanotroph abundance (Ab_{pred}) to offset the greater warming-induced methane production is therefore the abundance of methanotroph required to achieve the predicted 3.9-fold methane oxidation capacity in warmed pond sediment if the efficiency per methanotroph stays the same (i.e., 10.2 pmol CH_4 *pmoA*$^{-1}$h^{-1}).

In situ methane oxidation is limited by the diffusion of methane and oxygen. We acknowledge that by mixing the sediments and ^{13}C-CH_4 in our laboratory slurry measurements we would have optimized the

methane oxidation capacity in the sediments from both the warmed and ambient ponds. Therefore, we represent here, for the *ex situ* methane oxidation capacity, only the ratio between the warmed and ambient pond sediments (ratio W/A) to show that the kinetic effect and temperature effect increased the methane oxidation capacity by 1.9- and 1.4-fold in the warmed ponds relative to their ambient counterparts, respectively. In addition, if the depth of oxygen penetration serves as a proxy for active methanotrophy layer, altogether, the *ex situ* methane oxidation capacity in the warmed ponds would be 3.6-fold higher than in the ambient controls, close to the increase in methane production in the warmed ponds i.e. 3.7-fold, as well as the predicted amount of methane oxidized *in situ* i.e. 3.8-fold.

Supplementary Table 3 | Linear mixed-effect model results for the β-diversity analysis of *mcrA* library (*n*=79, monthly samples from April to August in 2016 from 8 ambient and 8 warmed ponds, *see* Methods)and *pmoA* library (*n*=80, monthly samples from March to July in 2017 from 8 ambient and 8 warmed ponds, *see* Methods).

The β-diversity was estimated using the scores along the first two principle coordinate axis (PCoA1 and PCoA2) of the Bray-Curtis distance measures. These were then fitted into a mixed-effects model with pond and sampling month treated as random effects. The statistical significance of the treatment (i.e., ambient or warmed ponds) was determined from the *F*-test using Satterthwaite's method for denominator degrees-of-freedom and *F*-statistic. The results were similar to a PERMANOVA analysis.

Treatment	PCoA1			PCoA2		
	% Variation[1]	F-value	P-value	% Variation[1]	F-value	P-value
mcrA	34.04	6.13	**<0.05**	22.93	3.54	**<0.10**
pmoA	46.20	0.037	0.85	13.89	0.46	0.51

[1]. The amount of variation captured in the axis is defined as the proportion of eigenvalue of that axis to the sum of all eigenvalues.

Supplementary Table 4 | Taxonomy assignment to the *mcrA* OTUs at 85 % identity (*n*=79, monthly samples from April to August in 2016 from 8 ambient and 8 warmed ponds, *see* Methods). Numbers in parentheses are standard errors.

Family	Genus	Sequence reads	
		Ambient	Warmed
Hydrogenotrophic methanogens			
unclustered *Methanomicrobiales*	unclustered *Methanomicrobiales*	227,766 (558)	225,753 (1,304)
Methanospirillaceae	*Methanospirillum*	256,777 (583)	184,696 (1,169)
Methanobacteriaceae	*Methanobacterium*	69,265 (210)	107,752 (398)
Methanomicrobiaceae	*Methanoplanus*	316 (3)	320 (7)
Methanomicrobiaceae	*Methanomicrobium*	174 (2)	223 (5)
Methanocellaceae	*Methanocella*	149 (3)	83 (2)
Methanothermaceae	*Methanothermus*	141 (1)	161 (2)
Methanocaldococcaceae	*Methanocaldococcus*	69 (1)	13 (0.3)
Methanobacteriaceae	*Methanothermobacter*	0 (0)	31 (1)
Methanomicrobiaceae	*Methanoculleus*	0 (0)	73 (2)
Acetoclastic methanogens			
Methanosaetaceae	*Methanosaeta*	257,132 (606)	287,992 (1,345)
Methanosarcinaceae	unclustered *Methanosarcinaceae*	7,285 (42)	5,071 (44)
Methylotrophic methanogens			
unclustered *Thermoplasmata*	unclustered *Thermoplasmata*	648 (7)	271 (7)
Methanosarcinaceae	*Methanohalophilus*	394 (4)	1,012 (8)
Methanoplasmatales	unclustered *Methanoplasmatales*	46 (1)	28 (1)
Methanosarcinaceae	*Methanosalsum*	0 (0)	25 (1)
Methanosarcinaceae	*Methanomethylovorans*	0 (0)	320 (8)

Supplementary Table 5 | Taxonomy assignment to the *pmoA* OTUs at 90 % identity (*n*=80, monthly samples from March to July in 2017 from 8 ambient and 8 warmed ponds, *see* Methods).
Highlighted warmed pond data were at a lower relative abundance in those ponds compared to the ambient ponds. Numbers in parentheses are standard errors.

Family	Genus	Sequence reads	
		Ambient	Warmed
Methylococcaceae	Type Ib	713,570 (1,689)	597,859 (1,081)
Methylocystaceae	*Methylocystis*	357,045 (1,166)	324,967 (855)
Methylocystaceae	Type IIa	4,784 (59)	100 (2)
MO3	unclustered MO3	2,532 (53)	1,681 (26)
Beijerinckiaceae	*Methylocapsa*-related	2,399 (37)	5 (0.1)
Environmental samples	Type IIb	2,012 (26)	79 (1)
Methylococcaceae	TUSC-like	1,062 (12)	14 (0.4)
Methylococcaceae	*Methylobacter*	1,372 (13)	158 (3)
Methylocystaceae	*Methylosinus*	535 (7)	1,848 (18)
unclustered *Proteobacteria*	unclustered Proteobacteria	362 (5)	0 (0)
pmoA-2	unclustered pmoA-2	235 (4)	410 (5)
Methylocystaceae	unclustered *Methylocystaceae*	166 (2)	88 (2)
unclustered *Rhizobiales*	unclustered *Rhizobiales*	149 (2)	12 (0.3)
Methylococcaceae	*Methylomonas*	13 (0.3)	0 (0)
unclustered *Methylococcales*	unclustered *Methylococcales*	0 (0)	181 (4)
Methylococcaceae	unclustered *Methylococcaceae*	0 (0)	28 (1)

Supplementary Table 6 | Multi-model selection for fitting generalized additive mixed effects models to the seasonal CH_4 emission data (*n*=3553 steady-state estimates, representing emissions from 7 ambient and 7 warmed ponds with each pond being notionally measured three times per day – *see* Methods).

To assess the effect of long-term warming on the median rate of methane emissions, a range of generalized additive mixed effects models (GAMMs) were fitted to the daily methane emission rate data (ME) as a function of treatment (i.e., warmed or ambient pond) and day of the year since 1st January 2017 (DOY). Whether the seasonal pattern of methane emissions differed between the treatment was also tested by comparing the smoother terms (DOY, by=Treatment) and s(DOY). Models were ranked using the AIC. ΔAIC refers to differences in AIC relative to the smallest AIC value and AIC weight is the probability of any model providing the best fit to the data e.g., 0.913 indicates that model (1) is the best fit to the data.

	Model	d.f.	AIC	ΔAIC	AIC Weight
(1)	Ln(ME)~Treatment+s(DOY,by=Treatment)	8	12035.0	0.00	0.913
(2)	Ln(ME)~s(DOY,by=Treatment)	7	12039.7	4.71	0.087
(3)	Ln(ME)~Treatment+s(DOY)	6	12194.2	159.24	0.000
(4)	Ln(ME)~s(DOY)	5	12198.9	163.94	0.000

A GAMM which included treatment on the intercept and a treatment-specified smoother term for DOY provided the best fit to the seasonal methane emission data, demonstrating an increase in median methane emission from warmed ponds as well as a difference in seasonality.

Supplementary Table 7 | Multi-model selection for fitting linear mixed-effect models to CH_4 potential production data (nmol CH_4 $g^{-1}h^{-1}$) as a function of treatment (e.g. warmed or ambient ponds), additional substrates and experimental incubation temperature (Ts) (*n*=662, sediment samples collected monthly and randomly from 3 to 5 of the 10 ambient and 3 to 5 of the 10 warmed ponds with each incubated at 3 temperatures and with up to 2 substrates. The sample size for control only, i.e., without additional substrates, of the total 662 samples, was 238. No replicate was applied within each pond.).

Ts represents the standardized temperature $\left(\frac{1}{kT_c}-\frac{1}{kT_{ij}}\right)$ in equation (4)**.** A range of linear mixed-effect models were fitted to the rate of methane production (ln(MG)) data. Note that only the fixed-effect parts of the models are included in the table. As in Supplementary Table 6, models were ranked using the AIC and an AIC weight of 0.76 indicates that model 1 is the best fit to the data.

	Model	d.f.	AIC	ΔAIC	AIC Weight
(1)	Ln(MG)~Ts+Treatment+Substrate +Ts×Treatment+Ts×Substrate +Treatment×Substrate	13	1820.6	0.00	0.76
(2)	Ln(MG)~Ts+Treatment+Substrate +Ts×Treatment+Ts×Substrate+ Treatment×Substrate+Ts×Treatment×Substrate	15	1823.4	2.78	0.19
(3)	Ln(MG)~Ts+Treatment+Substrate +Ts×Substrate+Treatment×Substrate	12	1826.3	5.71	0.04
(4)	Ln(MG)~Ts+Treatment+Substrate +Ts×Treatment+Ts×Substrate	11	1829.2	862	0.01
(5)	Ln(MG)~Ts+Treatment+Substrate+Ts×Substrate	10	1834.5	13.94	0.001

Note that in the incubations above 22°C the rate of CH_4 production plateaued and therefore we excluded these data from the model.

Supplementary Table 8 | Model selection procedure for fitting linear mixed-effect models to sediment methane potential production data (MG) as a function of carbon turnover *k* (*n*=32, sediment samples collected from 4 ambient and 4 warmed ponds in April, May, June and August, 2017).

The full model included additive terms and their interactions for two fixed effects – natural logarithm of carbon turnover *k* (lnk) and treatment type (i.e., ambient or warmed ponds). The significance (*p*-values) of the fixed-effect terms was determined using a likelihood ratio test on nested models. The *p*-value for comparing "Treatment×lnk" was 0.40, and the term removed from the model. As removing "Treatment×lnk" had no significant effect on model fit, model F1, that included a single slope but distinct intercepts provided the best fit to the methane potential data (marked in bold), demonstrating that the potential of sediments to produce methane increased equally in both the warmed and ambient pond sediments as carbon quality also increased but warming has stepped-up the fraction of carbon turned to methane.

Model	d.f.	AIC	LogLik	*p*-value
F0) ln(MG) ~ lnk×Treatment+lnk+Treatment	6	94.2	-41.09	
F1) ln(MG) ~ lnk + Treatment	**5**	**92.9**	**-41.44**	**0.40**
F2) ln(MG) ~ lnk	4	98.8	-45.4	<0.01
F3) ln(MG) ~ 1	3	107.7	-50.9	<0.001

Supplementary Table 9 | Model selection procedure for fitting mixed-effect models to methane oxidation as a function of kinetic or temperature responses.

a, Fitting Michaelis-Menten models to CH_4 oxidation rate (MO) as a function of initial CH_4 concentration (*n*=158, sediment samples collected from 8 ambient and 8 warmed ponds in July, 2017, and December, 2018, with a range of initial methane concentrations, *see* equation (7) in Methods). The full model included the initial methane concentrations (C_{CH4}) and the two Michaelis-Menten parameters defining the kinetic response, i.e., the maximum methane oxidation rate (V_{max}) and the Michaelis constant (K_m). The significance of treatment (i.e., warmed or ambient) on the parameters (V_{max} + Treatment) and (K_m + Treatment) was determined via Likelihood Ratio Test on nested models. As removing the effect of treatment on K_m and V_{max} had no significant effect on model fit (p=0.98 and p=0.45, respectively), the model with the same V_{max} and K_m terms for both warmed and ambient pond sediments provided the best fit to the CH_4 oxidation data (model F2, marked on bold).

Model	d.f.	AIC	LogLik	*p*-value
F0) MO ~ (C_{CH4}, V_{max}+Treatment, K_m+Treatment)	6	2106.21	-1047.10	
F1) MO ~ (C_{CH4}, V_{max} +Treatment, K_m)	5	2104.21	-1047.10	0.98
F2) MO ~ (C_{CH4}, V_{max}, K_m)	**4**	**2102.78**	**-1047.39**	**0.45**

b, Model selection procedure for fitting linear mixed-effect models to the temperature sensitivity of CH_4 oxidation rate (ln(MO)) (*n*=192, sediment samples collected from 8 warmed and 8 ambient ponds in May, June and July, 2017, incubated under four different temperatures). The full model included additive terms and their interactions for two fixed effects – standardized temperature at 15 °C (Ts, term $\left(\frac{1}{kT_C} - \frac{1}{kT_{ij}}\right)$ in equation (4)) and treatment type (i.e., ambient or warmed ponds). The significance of fixed-effect terms (p-values) were determined using a likelihood ratio test on nested models. For example, the significance of the term "Treatment×Ts", i.e., distinct slopes between warmed and ambient pond sediments, was determined by comparing nested model F0 to its reduced model F1. The p-value of this comparison was 0.24, the term "Treatment×Ts" was not significant and was thus removed from the model. As removing "Treatment×Ts" or "Treatment" had no significant effect on model fit, the model F2, that included a single slope and intercept, therefore provided the best fit to the CH_4 oxidation rate data (marked in bold), demonstrating that the CH_4 oxidation capacity and its temperature sensitivity were the same in both the warmed and ambient ponds.

Model	d.f.	AIC	LogLik	χ^2	*p*-value
F0) ln(MO)~Ts+Treatment×Ts+Treatment	8	287.12	-135.56		
F1) ln(MO)~Ts+Treatment	7	286.48	-135.56	1.36	0.24
F2) ln(MO)~Ts	**6**	**287.81**	**-137.91**	**3.33**	**0.068**
F3) ln(MO)~1	5	329.75	-159.88	43.94	<0.001

Supplementary Table 10 | Model selection procedure for fitting linear mixed-effect models to the carbon conversion efficiency (CCE) data.

a, Carbon conversion efficiency as function of temperature (*n*=191, sediment samples collected from 8 warmed and 8 ambient ponds in May, June and July, 2017, incubated under four different temperatures): The full model included additive terms and their interactions for two fixed effects – centered temperature at 15 °C (Tc, term $T - T_C$ in equation (8)) and treatment types (i.e., ambient or warmed ponds). The significance (*p*-values) of fixed-effect terms was determined using a likelihood ratio test on nested models. As removing "Treatment×Tc" or "Treatment" had no significant effect on model fit, the model, F2, that included one common slope and intercept provided the best fit to CCE data (marked in bold).

Model	d.f.	AIC	LogLik	χ^2	*p*-value
F0) CCE~Tc+Treatment+ Treatment×Tc	8	1041.2	-512.61		
F1) CCE~Tc+Treatment	7	1039.5	-512.72	0.23	0.63
F2) CCE~Tc	**6**	**1037.7**	**-512.84**	**0.23**	**0.63**
F3) CCE~1	5	1069.0	-529.51	33.34	<0.01

b, Carbon conversion efficiency as function of methane concentration (*n*=69, sediment samples collected in July, 2017, from 8 ambient and 8 warmed ponds with a range of initial methane concentrations): The full model included additive terms and their interactions for two fixed effects – initial $^{13}C\text{-}CH_4$ concentration (C_{CH4}, *see* equation (9)) and treatment type (i.e., ambient or warmed ponds). The significance (*p*-value) of fixed-effect terms was determined using a likelihood ratio test on nested models. As removing "C_{CH4}×Treatment" or "Treatment" had no significant effect on model fit, the model, F2, that included one common slope and intercept provided the best fit to CCE data (marked in bold).

Model	d.f.	AIC	LogLik	χ^2	*p*-value
F0) CCE~C_{CH4}+Treatment+ C_{CH4}×Treatment	6	458.78	-223.39		
F1) CCE~C_{CH4}+Treatment	5	456.86	-223.43	0.083	0.77
F2) CCE~C_{CH4}	**4**	**455.63**	**-223.82**	**0.77**	**0.38**
F3) CCE~1	3	463.93	-228.97	10.30	<0.01

Supplementary References

1. Inglett, K. S., Inglett, P. W., Reddy, K. R. & Osborne, T. Z. Temperature sensitivity of greenhouse gas production in wetland soils of different vegetation. *Biogeochemistry* **108**, 77–90 (2012).
2. Hodgkins, S. B. *et al.* Changes in peat chemistry associated with permafrost thaw increase greenhouse gas production. *Proc. Natl. Acad. Sci. U. S. A.* **111**, 5819–5824 (2014).
3. Valentine, D. W., Holland, E. A. & Schimel, D. S. Ecosystem and physiological controls over methane production in northern wetlands. *J. Geophys. Res. Atmos.* **99**, 1563–1571 (1994).
4. Tfaily, M. M. *et al.* Journal of Geophysical Research: Biogeosciences. *J. Geophys. Res. Biogeosciences* **119**, 661–675 (2014).
5. Wright, E. L. *et al.* Contribution of subsurface peat to CO_2 and CH_4 fluxes in a neotropical peatland. *Glob. Chang. Biol.* **17**, 2867–2881 (2011).
6. Updegraff, K., Pastor, J., Bridgham, S. D. & Johnston, C. A. Environmental and substrate controls over carbon and nitrogen mineralization in northern wetlands. *Ecol. Appl.* **5**, 151–163 (1995).
7. Blodau, C. & Deppe, M. Humic acid addition lowers methane release in peats of the Mer Bleue bog, Canada. *Soil Biol. Biochem.* **52**, 96–98 (2012).
8. Kolton, M., Marks, A., Wilson, R. M., Chanton, J. P. & Kostka, J. E. Impact of warming on greenhouse gas production and microbial diversity in anoxic peat from a Sphagnum-dominated bog (Grand Rapids, Minnesota, United States). *Front. Microbiol.* **10**, 1–13 (2019).
9. Hodgkins, S. B. *et al.* Soil incubations reproduce field methane dynamics in a subarctic wetland. *Biogeochemistry* **126**, 241–249 (2015).
10. Keller, J. K. & Bridgham, S. D. Pathways of anaerobic carbon cycling across an ombrotrophic-minerotrophic peatland gradient. *Limnol. Oceanogr.* **52**, 96–107 (2007).
11. Bridgham, S. D., Johnston, C. A., Pastor, J. & Updegraff, K. Potential Feedbacks of Northern Wetlands on Climate Change. *Bioscience* **45**, 262–274 (1995).
12. McCalley, C. K. *et al.* Methane dynamics regulated by microbial community response to permafrost thaw. *Nature* **514**, 478–481 (2014).
13. Glissmann, K., Chin, K. J., Casper, P. & Conrad, R. Methanogenic pathway and archaeal community structure in the sediment of eutrophic Lake Dagow: Effect of temperature. *Microb. Ecol.* **48**, 389–399 (2004).
14. Keller, J. K., Weisenhorn, P. B. & Megonigal, J. P. Humic acids as electron acceptors in wetland decomposition. *Soil Biol. Biochem.* **41**, 1518–1522 (2009).
15. Fey, A. & Conrad, R. Effect of Temperature on Carbon and Electron Flow and on the Archaeal Community in Methanogenic Rice Field Soil. *Appl. Environ. Microbiol.* **66**, 4790–4797 (2000).
16. Sonnentag, O. & Quinton, W. L. AmeriFlux CA-SCB Scotty Creek Bog. (2016) doi:10.17190/AMF/1498754.
17. Chen & Jiquan. AmeriFlux US-CRT Curtice Walter-Berger cropland. (2016) doi:10.17190/AMF/1246156.
18. Schuur & Ted. AmeriFlux US-EML Eight Mile Lake Permafrost thaw gradient, Healy Alaska. (2018) doi:10.17190/AMF/1418678.
19. Krauss & Ken. AmeriFlux US-LA1 Pointe-aux-Chenes Brackish Marsh. (2016) doi:10.17190/AMF/1543386.
20. Krauss & Ken. AmeriFlux US-LA2 Salvador WMA Freshwater Marsh. (2016) doi:10.17190/AMF/1543387.
21. Desai & Ankur. AmeriFlux US-Los Lost Creek. (2016) doi:10.17190/AMF/1246071.
22. Baldocchi & Dennis. AmeriFlux US-Myb Mayberry Wetland. (2016) doi:10.17190/AMF/1246139.
23. Bohrer & Gil. AmeriFlux US-ORv Olentangy River Wetland Research Park. (2016) doi:10.17190/AMF/1246135.
24. Bohrer & Gil. AmeriFlux US-OWC Old Woman Creek. (2018) doi:10.17190/AMF/1418679.

25. Desai & Ankur. AmeriFlux US-PFa Park Falls/WLEF. (2016) doi:10.17190/AMF/1246090.
26. Baldocchi & Dennis. AmeriFlux US-Sne Sherman Island Restored Wetland. (2018) doi:10.17190/AMF/1418684.
27. Vargas & Rodrigo. AmeriFlux US-StJ St Jones Reserve. (2016) doi:10.17190/AMF/1480316.
28. Baldocchi & Dennis. AmeriFlux US-Tw1 Twitchell Wetland West Pond. (2016) doi:10.17190/AMF/1246147.
29. Baldocchi & Dennis. AmeriFlux US-Tw4 Twitchell East End Wetland. (2016) doi:10.17190/AMF/1246151.
30. Baldocchi & Dennis. AmeriFlux US-Twt Twitchell Island. (2016) doi:10.17190/AMF/1246140.
31. Iwata, H., Ueyama, M. & Harazono, Y. AmeriFlux US-Uaf University of Alaska, Fairbanks. (2016) doi:10.17190/AMF/1480322.
32. Chen & Jiquan. AmeriFlux US-WPT Winous Point North Marsh. (2016) doi:10.17190/AMF/1246155.